An Improved Remote Sensing Image Fusion Algorithm Based on IHS Transformation

Chao Deng[1], Zhi-heng Wang[2], Xing-wang Li[1], Hui-na Li[1] and Charles C. Cavalcante[3]
[1] School of Physics and Electronic Information Engineering, Henan Polytechnic University
Jiaozuo, 454000 China
[e-mail: super@hpu.edu.cn]
[2] Computer Science and Technology, Henan Polytechnic University
Jiaozuo, 454000 China
[3] Wireless Telecommunications Research Group, Federal University of Ceará
Campus do Pici, Bl. 722, ZIP 60455-760, Fortaleza-CE, Brazil
[e-mail: charles@gtel.ufc.br]
*Corresponding author: Charles C. Cavalcante

Received May 7, 2016; revised November 10, 2016; revised December 14, 2016; accepted January 22, 2017; published March 31, 2017

Abstract

In remote sensing image processing, the traditional fusion algorithm is based on the Intensity-Hue-Saturation (IHS) transformation. This method does not take into account the texture or spectrum information, spatial resolution and statistical information of the photos adequately, which leads to spectrum distortion of the image. Although traditional solutions in such application combine manifold methods, the fusion procedure is rather complicated and not suitable for practical operation. In this paper, an improved IHS transformation fusion algorithm based on the local variance weighting scheme is proposed for remote sensing images. In our proposal, firstly, the local variance of the SPOT (which comes from French "Systeme Probatoire d'Observation dela Tarre" and means "earth observing system") image is calculated by using different sliding windows. The optimal window size is then selected with the images being normalized with the optimal window local variance. Secondly, the power exponent is chosen as the mapping function, and the local variance is used to obtain the weight of the I component and match SPOT images. Then we obtain the I' component with the weight, the I component and the matched SPOT images. Finally, the final fusion image is obtained by the inverse Intensity-Hue-Saturation transformation of the I', H and S components. The proposed algorithm has been tested and compared with some other image fusion methods well known in the literature. Simulation result indicates that the proposed algorithm could obtain a superior fused image based on quantitative fusion evaluation indices.

Keywords: Intensity-Hue-Saturation transformation, spectrum distortion, local variance weight, image fusion, multi-spectral images

This work is supported by the National Natural Science Foundation of China (61572173, 61472119 and 61472373), and Henan Polytechnic University Innovative Research Team (T2014-3).

https://doi.org/10.3837/tiis.2017.03.021 **ISSN : 1976-7277**

1. Introduction

With the rapid development of data communication, sensor and remote sensing technology, image resources are now displaying increased diversity and complexity. Since there exist limitations when characterizing a target with data from a single sensor, image fusion technology has been employed to cope with this issue [1-7]. A general definition of data fusion can be adopted as fallowing: "Data fusion is a formal framework which expresses means and tools for the alliance of data originating from different sources. It aims at obtaining information of greater quality; the exact definition of 'greater quality' will depend upon the application" [8-10]. Some fusion technology has been used in sensed image analysis and got good results. With the development of remote sensing techniques, it is very important to acquire more complete and more reliable data by combining multi-source remote sensing data [11-12]. The purpose of image fusion is to reduce ambiguity and minimize redundancy in the output while maximizing the relative information specific to an application [13-21].

The fused images made by the traditional intensity-hue-saturation (IHS) transformation have improved the clarity of the images while retaining the high resolution, tone and saturation from the original ones. However, the *I* component of the original image is replaced with SPOT image by histogram match directly, which lead to the information's missing. The texture information and spectrum, spatial resolution and statistical information of the images are not adequately taken into consideration, which might result in spectral distortion [22-24]. In addition, although traditional solutions combine manifold methods, yet it is rather complicated and not suitable for practical use. A new method is proposed in [8], which aims at finding a transformation of the original space that would produce such new features, which preserve or improve as much as possible. It adds the I* to form a fused intensity component with the low frequency information from the low resolution MS image and the edge of PAN image. In our paper, we do not just focus on improving some parameters, because some parameters getting better will result in other parameters getting worse, the better balance among the parameters is the key to get better fusion result. Obtaining the best cost performance is very important to get the better balance.

In this paper, an improved IHS fusion algorithm based on local variance weighting scheme is proposed in this paper. The new algorithm incorporates the local variance weight, the high frequency information (SPOT image) and the low frequency information (I component) can be changed and kept adaptively with the different area, the more information can be kept. Simulation result indicates that the proposed algorithm results in a superior fused image based on quantitative fusion evaluation indices.

The rest of the paper is organized as follows. Section 2 reviews the traditional IHS transformation method for image fusion while in Section 3, the improved IHS fusion algorithm based on local variance weighting scheme is introduced. Section 4 presents experimental and simulated performance of the algorithm and finally, conclusions are stated in Section 5.

2. Traditional IHS Transformation Algorithm

The IHS transformation mode is embedded with two important characteristics. First, the *I* component is independent of the color component. Second, the *H* component and *S* component are closely related to human color perception [25-26].

There are many kinds of IHS transformation and its inverse transformation, among which sphere transformation, cylinder transformation, triangle transformation and single six pyramid transformation are the most commonly used [27-28]. Being advantageous in easy computation, the triangle transformation becomes the most extensively applied algorithm and is therefore chosen in this paper and can be expressed as:

$$\begin{bmatrix} I \\ V_1 \\ V_2 \end{bmatrix} = \begin{bmatrix} \frac{1}{\sqrt{3}} & \frac{1}{\sqrt{3}} & \frac{1}{\sqrt{3}} \\ \frac{1}{\sqrt{6}} & \frac{1}{\sqrt{6}} & -\frac{2}{\sqrt{6}} \\ \frac{1}{\sqrt{2}} & -\frac{1}{\sqrt{2}} & 0 \end{bmatrix} \times \begin{bmatrix} R \\ G \\ B \end{bmatrix}, \tag{1}$$

$$H = \arctan\left(\frac{V_1}{V_2}\right), \tag{2}$$

$$S = \sqrt{V_1^2 + V_2^2}\ . \tag{3}$$

The triangle inverse transformation is given by:

$$\begin{bmatrix} R \\ G \\ B \end{bmatrix} = \begin{bmatrix} \frac{1}{\sqrt{3}} & \frac{1}{\sqrt{6}} & \frac{1}{\sqrt{2}} \\ \frac{1}{\sqrt{3}} & \frac{1}{\sqrt{6}} & -\frac{1}{\sqrt{2}} \\ \frac{1}{\sqrt{3}} & -\frac{2}{\sqrt{6}} & 0 \end{bmatrix} \times \begin{bmatrix} I \\ V_1 \\ V_2 \end{bmatrix}, \tag{4}$$

where V_1 and V_2 are two intermediate values.

3. The improved IHS transformation based on local variance weighting scheme

The traditional IHS transformation transforms the landsat Thematic Mapper (TM) image from RGB to IHS, and replaces the *I* component with SPOT image by histogram match, then obtains the fusion result by IHS inverse transformation. The *I* component of the original image is replaced directly, which lead to the information's missing. So this method does not take into account the texture and spectrum information, spatial resolution and statistical information of the photos adequately, and results in the image spectrum distortion. If the high frequency information (SPOT image) and the low frequency information (*I* component) can be changed and kept adaptively with the different area, the fusion result will be better. The image's local variance is an important parameter to local spectral information of the image, the local variance value is big in regions with large change of local spectral information, which mean the high frequency information (SPOT image) is more and should be considered to keep more. On the contrary, if the local variance value is small, spectral homogeneity regions of the image have more low frequency information (I component) which should be kept more. So the

proposed algorithm in this paper incorporates the local variance weight, and the basic principle is that if the local area has a large local variance, then the weight of the high frequency information (SPOT image) should be large, and the weight of the low frequency information (*I* component) should be small. On the contrary, if the local area has a small local variance, the weight of the high frequency information (SPOT image) should be small, and the weight of the low frequency information (*I* component) should be large. The sum of the two weights is kept to be 1. The goal is to get more information and better fusion result. The improved method contains the following steps:

(1) Calculate the local variance of the SPOT images with different windows, analyze and select the optimal size of the window with the experiment;

(2) Normalize the images with the best window local variance to establish the relationship between the image and the weight;

(3) Transform 3 band data of the TM image from RGB space to IHS space and obtain the I, H, and S components;

(4) Match the SPOT images by histogram based on the I component;

(5) By using power exponent as mapping functions, establish the weight of the I component and the matched SPOT images, which can help to get the more accurate component;

(6) Build the I' component with the weight, the I component and the matched SPOT images, the I' component has more information and can make the fusion result better;

(7) Obtain the final fusion image using the IHS inverse transformation of I', H and S. The main flow chart of the method is shown as follows:

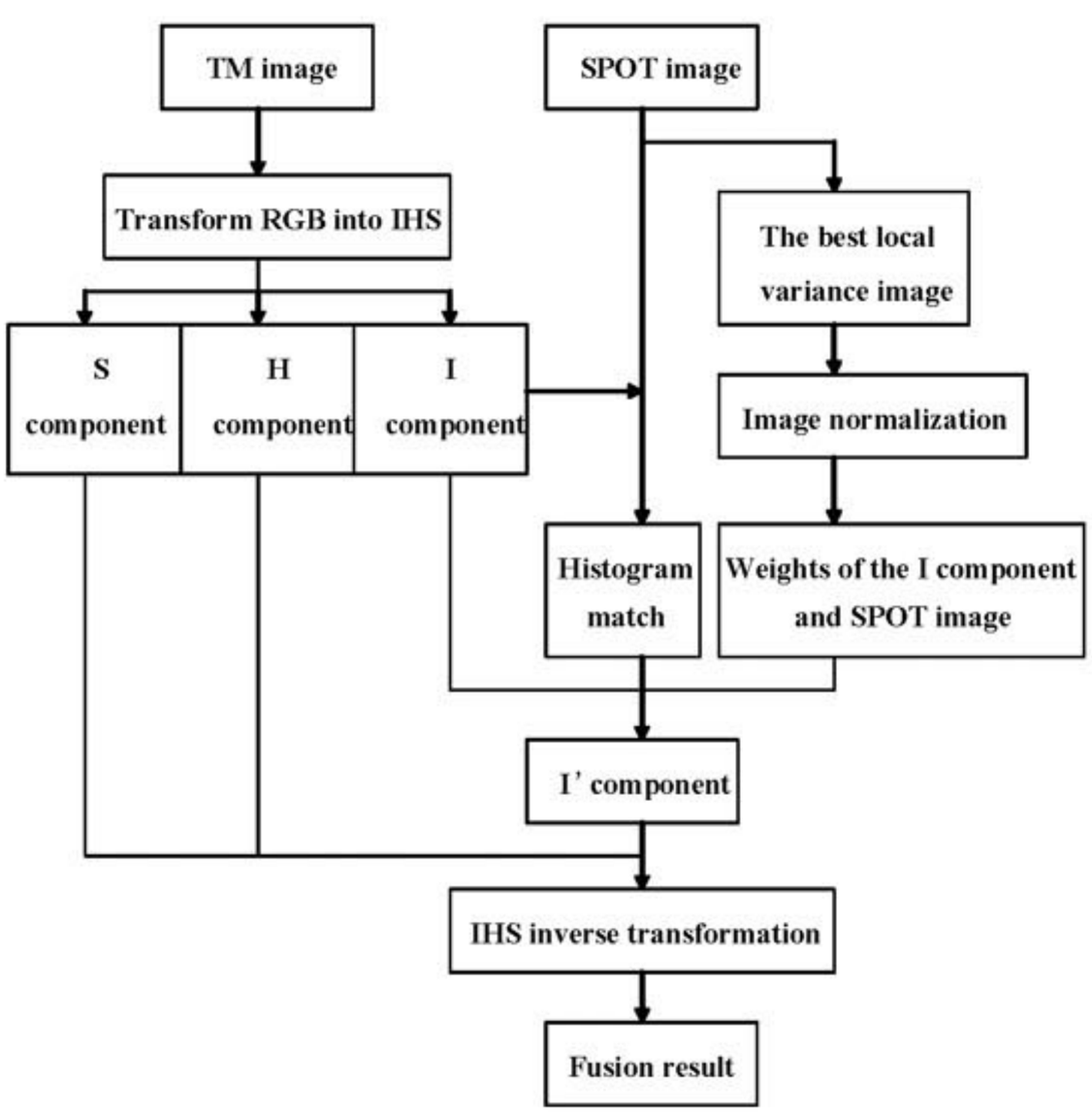

Fig. 1. Flow chart of the improved algorithm fusion.

3.1 Choose the SPOT image with the best local variance

A proper sliding window is important for calculating the local variance of the image. A large window can guarantee that the texture classification of the surface feature is representative, but it may contain extraneous information and cause blurring at the edge of the surface feature. In contrast, a small window can not describe the distribution regulation of the surface feature completely and accurately [29-30]. In our experiment, four kinds of windows (3×3, 5×5, 7×7 and 9×9) are tested to determine the best sliding window in terms of the mean, standard deviation, information entropy and average gradient [31].

Mean. The mean of an image represents the averaged value of all pixels. The visual effect is the best if the mean is moderate (about 128 in gray scale) and the mean can be calculated as:

$$\mu = \frac{1}{MN}\sum_{i=1}^{M}\sum_{j=1}^{N}F(i,j), \tag{5}$$

where $F(i,j)$ is the value of pixel with x coordinate i and y coordinate j, while M and N are the width and height of the image,respectively.

Standard Deviation. The standard deviation indicates the degree of dispersion of pixel values. Large standard deviation means higher image contrast, which implies better visual effect. The standard deviation (std), is given by:

$$std = \sqrt{\frac{\sum_{i=1}^{M}\sum_{j=1}^{N}(F(i,j)-\mu)^2}{MN}}. \tag{6}$$

Entropy. According to Shannon information theory, proposed in 1948, the entropy quantifies the average amount of information. Higher entropy means better visual effect and the entropy, H, can be calculated as:

$$H = -\sum_{i=0}^{L-1}P_i logP_i, \tag{7}$$

where L is the image grayscale, P_i is the probability of occurrence of a pixel with a grayscale of i.

Average gradient. Average gradient reflects the image clarity and is given by:

$$\bar{G} = \frac{1}{MN}\sum_{i=1}^{M}\sum_{j=1}^{N}\sqrt{\frac{\Delta F_x^2+\Delta F_y^2}{2}}, \tag{8}$$

$$\Delta F_x = F(i+1,j)-F(i,j), \tag{9}$$

$$\Delta F_y = F(i+1,j)-F(i,j), \tag{10}$$

where ΔF_x and ΔF_y are the disparity of the X and Y direction. The bigger the average gradient, the better the image clarity.

A SPOT image and TM image (**Fig. 9** - a, b) are selected to test the method in this paper. The experimental result is shown below in **Fig. 2**:

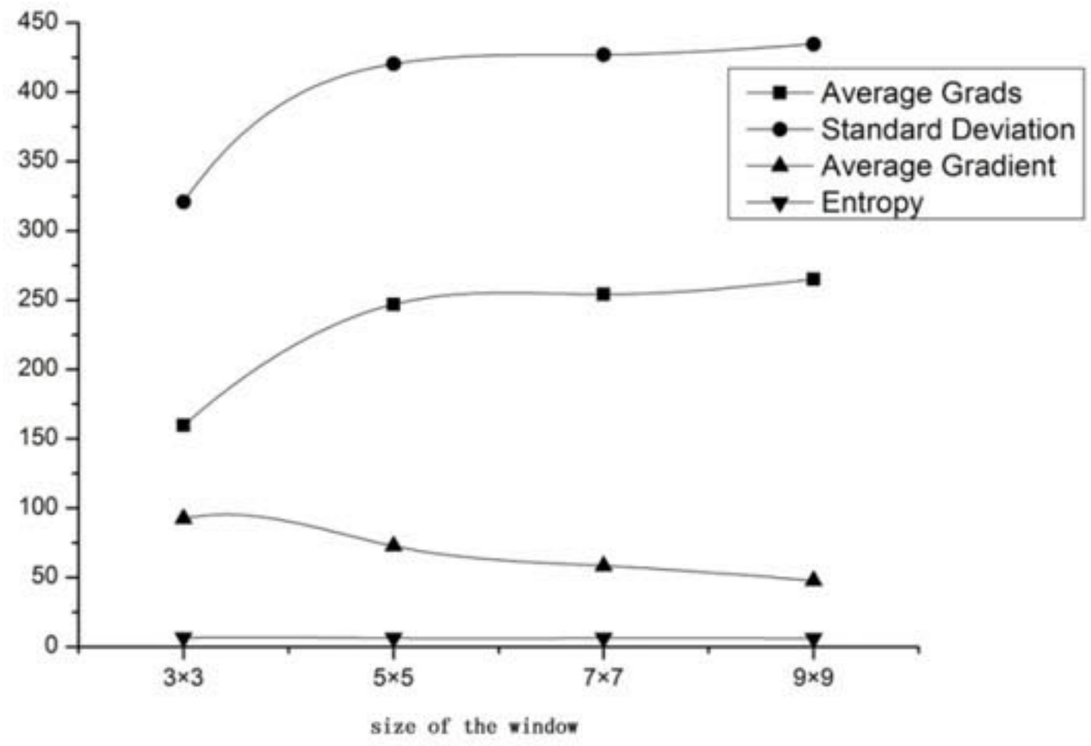

Fig. 2. The relationship between statistical characteristics of the images and the window size.

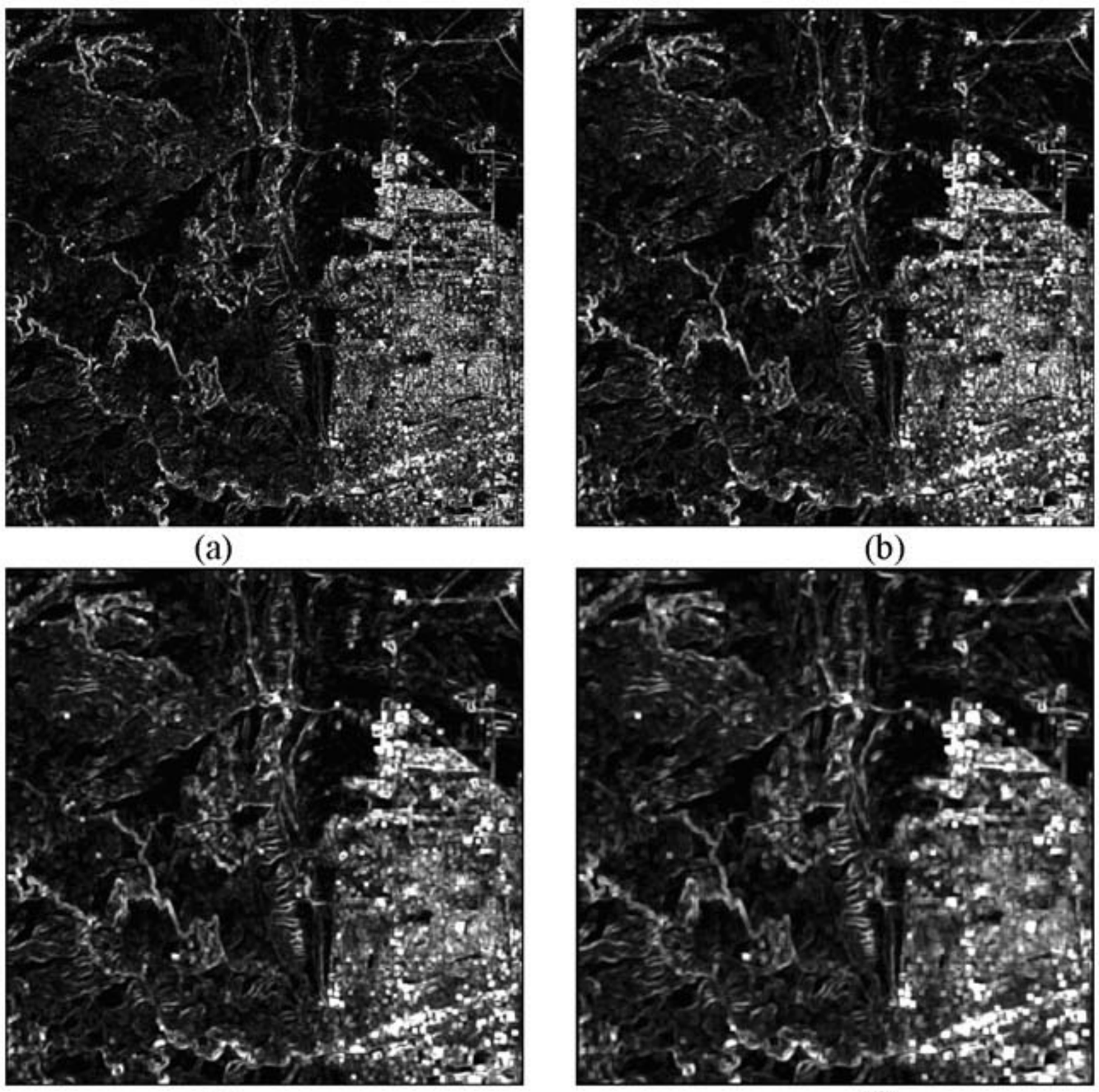

Fig. 3. Local standard deviation images of the different sizes of sliding window (a) 3×3 window (b) 5×5 window (c) 7×7 window (d) 9×9 window

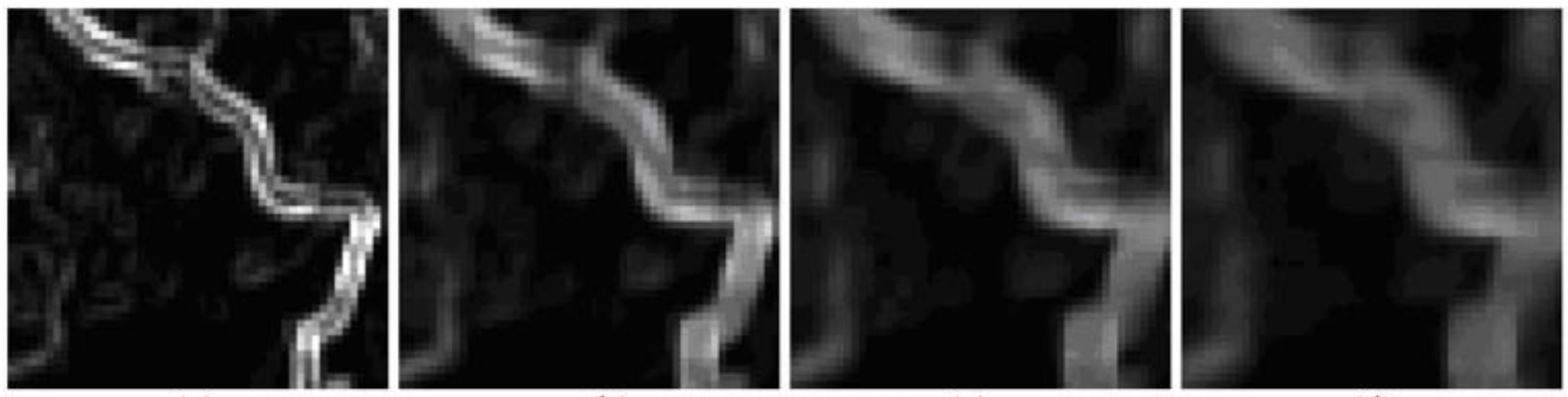

(a) (b) (c) (d)

Fig. 4. Local amplified standard deviation images of the different sizes of sliding window. (a) 3×3 window (b) 5×5 window (c) 7×7 window (d) 9×9 window

From **Fig. 2**, we can find that both mean and standard deviation increase with the sizes of the window while the average gradient and entropy decrease. The best values can be obtained for four parameters when the size of the window is 5×5. As can be seen in **Fig. 3** and **Fig. 4**, a 5×5 sliding window could keep the edge information and statistical characteristics, and it is chosen for the best local variance. The 5×5 sliding window is not coming from one dataset, many experiments has proven the 5×5 sliding window size is optical. The optical window size chooses on the two aspects, one is the relationship between statistical characteristics of the images and the window size, the other is the visual judgement.

3.2 Normalization of the best window image

Because the local variance range changes with the different image, the weight of the high frequency information and low frequency information stays between 0 and 1, so, in order to build the weight of the different variance images and the I component and SPOT image, normalization of the local variance image with the 5×5 window is chosen, and the image value range stays between 0 and 1.The following formula is used for normalization:

$$P=\frac{DN-DN_{min}}{DN_{max}-DN_{min}}, \tag{11}$$

where DN is the gray value of image, DN_{max} and DN_{min} are, respectively, the maximum and minimum gray value of the window image.

3.3 Histogram matching

Being an important step of the IHS fusion, histogram matching can alleviate the spectrum characteristic distortion caused by the spectral response in different ranges, and it could also reduce the influence of the illuminating condition, the angle of the sun, the viewing angle and the terrain fluctuation. Besides, histogram matching can guarantee better consistency of the spectral characteristics of the multi-source remote sensing image [32-34]. Based on the I component histogram, the SPOT images are matched by histogram with the Environment for Visualizing Images (ENVI). Histogram matching makes the intensity of the two images as close as possible. An example of histogram matching is shown in **Fig. 5**.

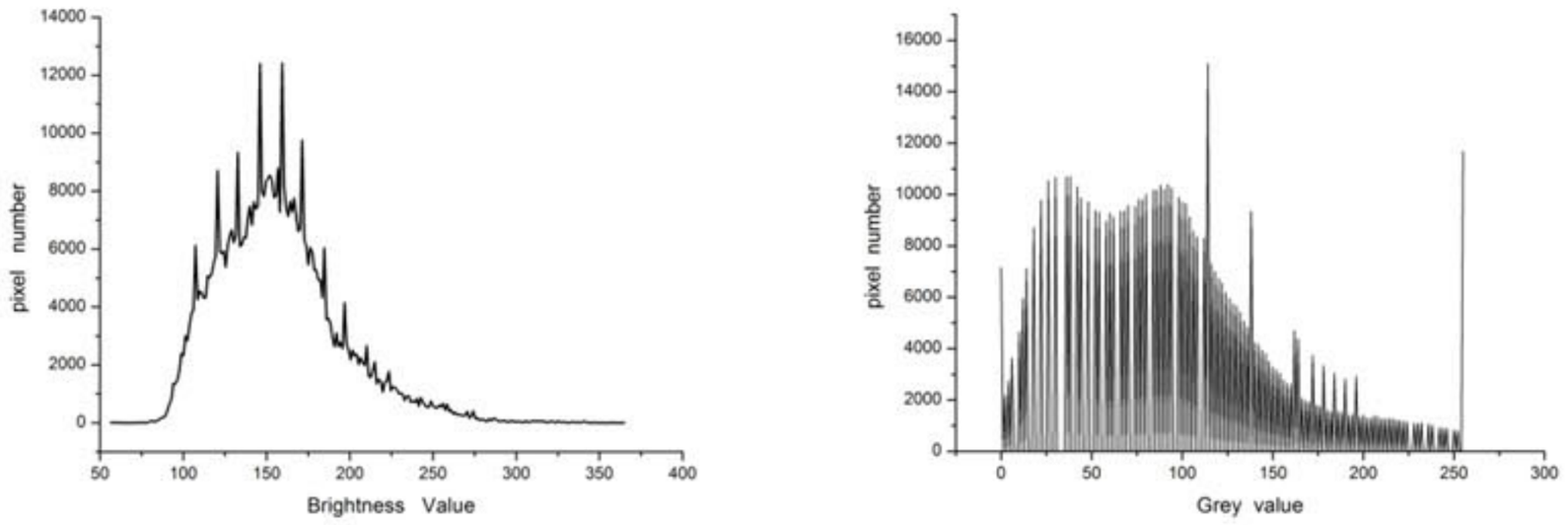

(a) (b)

Fig. 5. Histogram matching results of the images.
(a) the histogram of *I* component (b) the histogram matching results of SPOT

3.4 Weight image acquisition

After the normalization, it is important to link the local variance to the *I* component and the SPOT image which is matched by histogram. In this paper, the power exponent is chosen as the mapping function, and the local variance is chosen as the weight. The detailed procedures are given as follows:

(1) Choose Y as the weight of the SPOT image, choose X as the local variance after normalization;

(2) Set $Y = X^N$, where $N = 1, 1/25, 1/50, 1/75, 1/100, 1/125$ and $1/150$.

The weight of the I component is therefore $1-Y$, the I' component is computed as follows:

$$I' = Y \times SPOT + (1-Y) \times I \,. \tag{12}$$

4. Experimental Results and Performance Evaluation

4.1 The analysis and evaluation of the experimental result

The evaluation indicator of the fusion images, based on different value of mapping function (power exponent), is shown below:

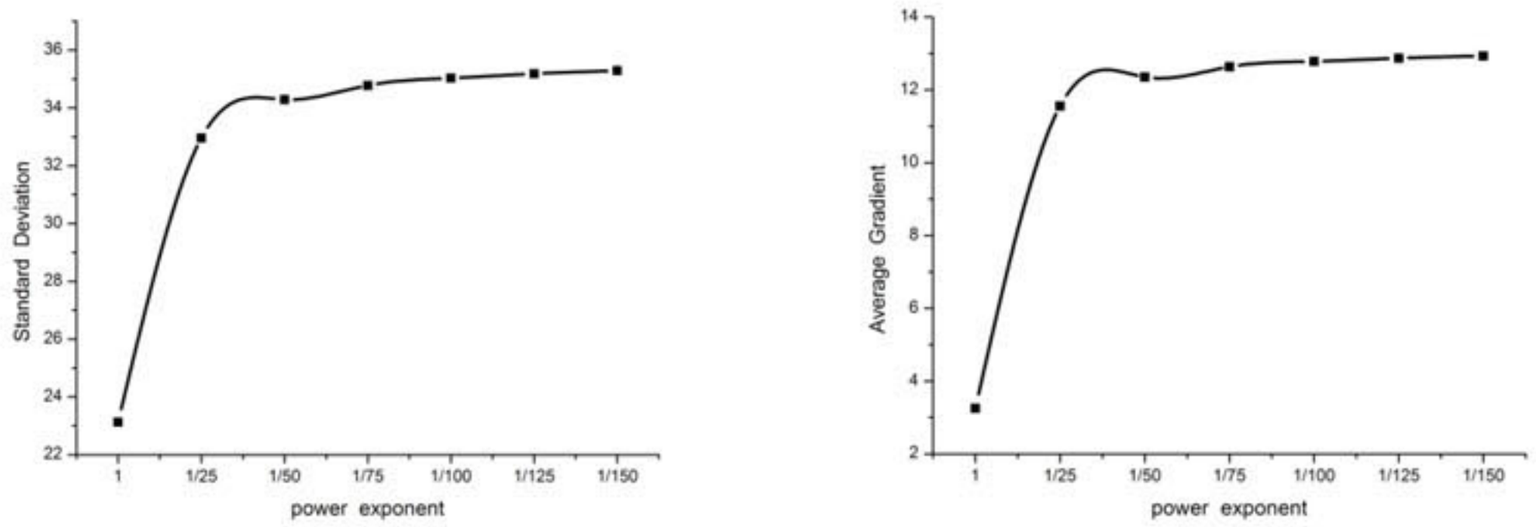

(a) (b)

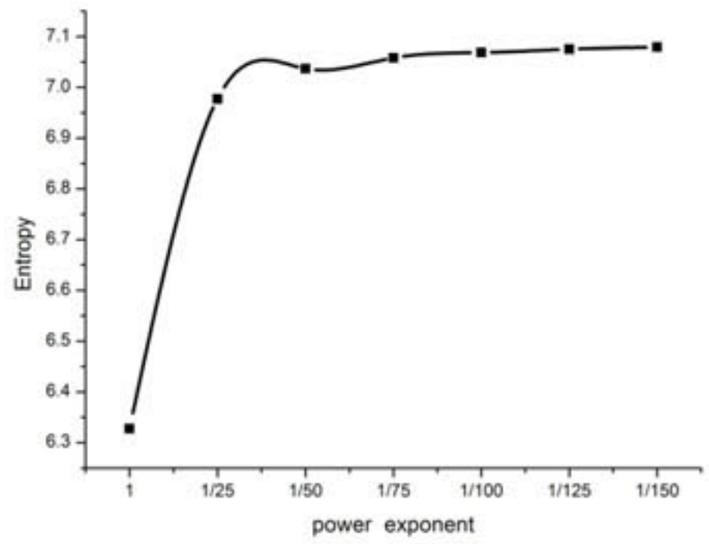

(c)

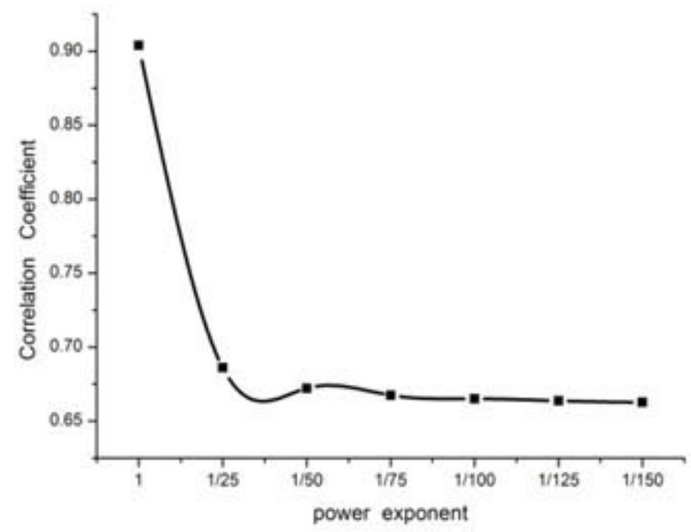

(d)

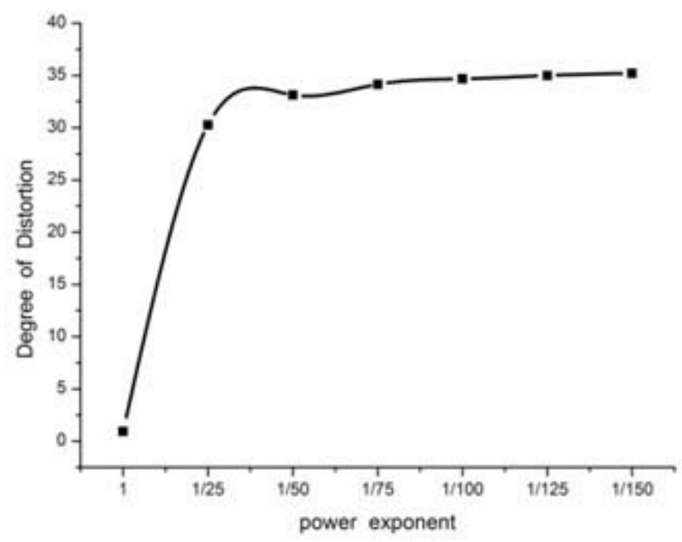

(e)

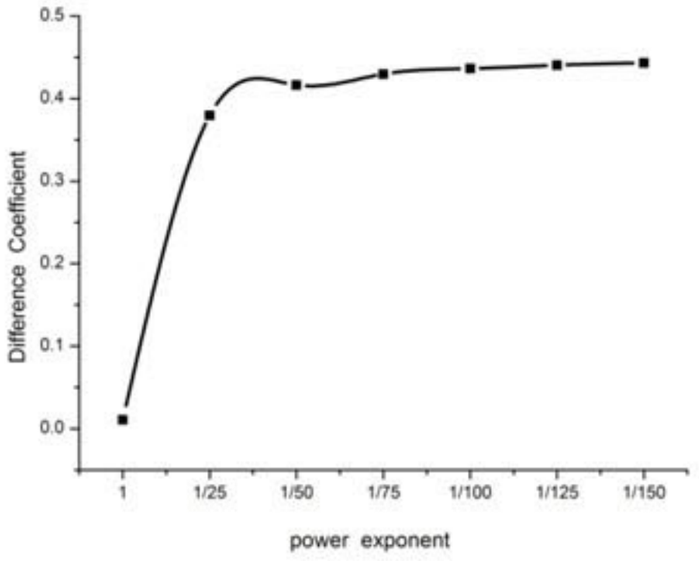

(f)

Fig. 6. Evaluation index tendency chart of fusion results: (a) The variation trend of standard deviation; (b) Thevariation trend of average gradient; (c) The variation trend of entropy; (d) The variation trend of correlation coefficient; (e) The variation trend of distortion degree; (f) The variation trend of difference coefficient.

According to the figures of the evaluation indices, the variation rule can be described as: with the decrease of the power exponent, the average gradient, entropy and standard deviation of the fusion images increase while the correlation coefficient of the images, the distortion degree and the difference coefficient decrease.

According to the analysis of the above evaluation indices, the increase of the average gradient, standard deviation and entropy will result in the reduction of the spectrum fidelity (difference coefficient, distortion degree and correlation coefficient). Therefore, an appropriate power exponent with the highest cost performance is the key to the fusion.

Comparison to the traditional IHS transformation in terms of those indices can be described using two equations.

(1) Comparison in terms of clarity, standard deviation, informationentropy and correlation coefficient can be described as:

$$L_i = \frac{M_i - N_i}{N_i}, \tag{13}$$

where L_i stands for the variation relative to the traditional IHS fusion result, N_i represents the traditional IHS index, M_i represents the improved fusion index with i = 1, 2, 3 and 4 corresponding to clarity, standard deviation, information entropy, and correlation coefficient,

respectively.

(2) Comparison in terms of the difference coefficient and distortion degree can be described as:

$$C_i = \frac{Q_i - P_i}{Q_i}, \tag{14}$$

where C_i represents the variation relative to the traditional IHS fusion result, Q_i represents the traditional IHS index, P_i represents the improved fusion index, with i = 1 and 2 corresponding to difference coefficient and distortion degree.

The index variation of the images is shown in Table 1. Where SD represents the standard deviation, AG represents average gradient, IE represents the information entropy, DD represents the distortion degree, DC represents the difference coefficient and CC stands for the correlation coefficient. In the rest of the paper, they keep the same meaning.

The selected application lists for each class and the number of applications in each class are shown in Table 1.

Table 1. Applications in each class

MappingFunction Y=	S D	A G	I E	D D	D C	C C
X	-0.4643	-0.7338	-0.1355	0.9925	0.9916	0.3693
$X^{\frac{1}{25}}$	-0.1326	-0.1653	-0.0289	0.2186	0.2236	0.0656
$X^{\frac{1}{50}}$	-0.0731	-0.0876	-0.0153	0.1211	0.1239	0.0330
$X^{\frac{1}{75}}$	-0.0510	-0.0593	-0.0105	0.0857	0.0875	0.0220
$X^{\frac{1}{100}}$	-0.0395	-0.0446	-0.0081	0.0675	0.0690	0.0164
$X^{\frac{1}{125}}$	-0.0325	-0.0357	-0.0066	0.0563	0.0577	0.0131
$X^{\frac{1}{150}}$	-0.0277	-0.0296	-0.0056	0.0488	0.0498	0.0109

In order to obtain the best cost performance, the variation of the six indices is taken into account using the following equation:

$$Y = \frac{A + B + C}{D + E + F}, \tag{15}$$

where A, B, C, D, E and F stand for the standard variance, average gradient, information entropy, distortion degree, difference coefficient and correlation coefficient, respectively.

4.2 The obtainment of the power exponent

The coarse range of the power exponent has been obtained in Section4.1, while its fine range requires the use of the Interactive Data Language (IDL). Cost performance tendency chart of fusion results is shown in Fig. 7. The detailed procedures are described as follows and also shown in Fig. 8, where "value of 1/X" stands for the values of cost performance when the power exponent is 1/X for simplicity.

(1) The values of 1/24 and 1/26 are calculated. If both values are smaller than that of 1/25,

the best power exponent is 1/25;

(2) If the value of 1/24 is larger than that of 1/25, while the value of 1/25 is larger than that of 1/26, the value of 1/23 will be calculated and compared with the value of 1/24. If the value of 1/23 is smaller than that of 1/24, the best power exponent is 1/24. Otherwise, the value of 1/22 will be calculated and compared until the largest value point is found.

(3) If the value of 1/26 is larger than that of 1/25, while the value of 1/25 is larger than that of 1/24, the value of 1/27 will be calculated and compared with the value of 1/26. If the value of 1/27 is smaller than that of 1/26, then the best power exponent is 1/26. Otherwise, the value of 1/28 will be calculated and compared until the largest value point is found.

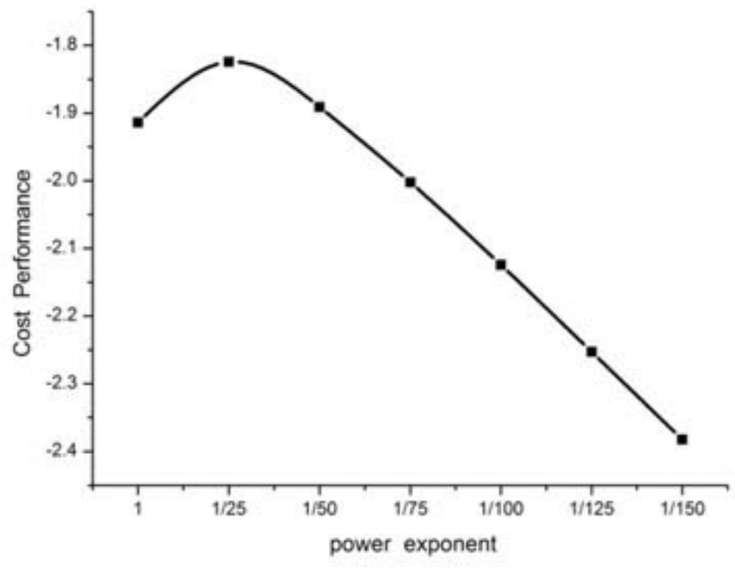

Fig. 7. Cost performance tendency chart of fusion results.

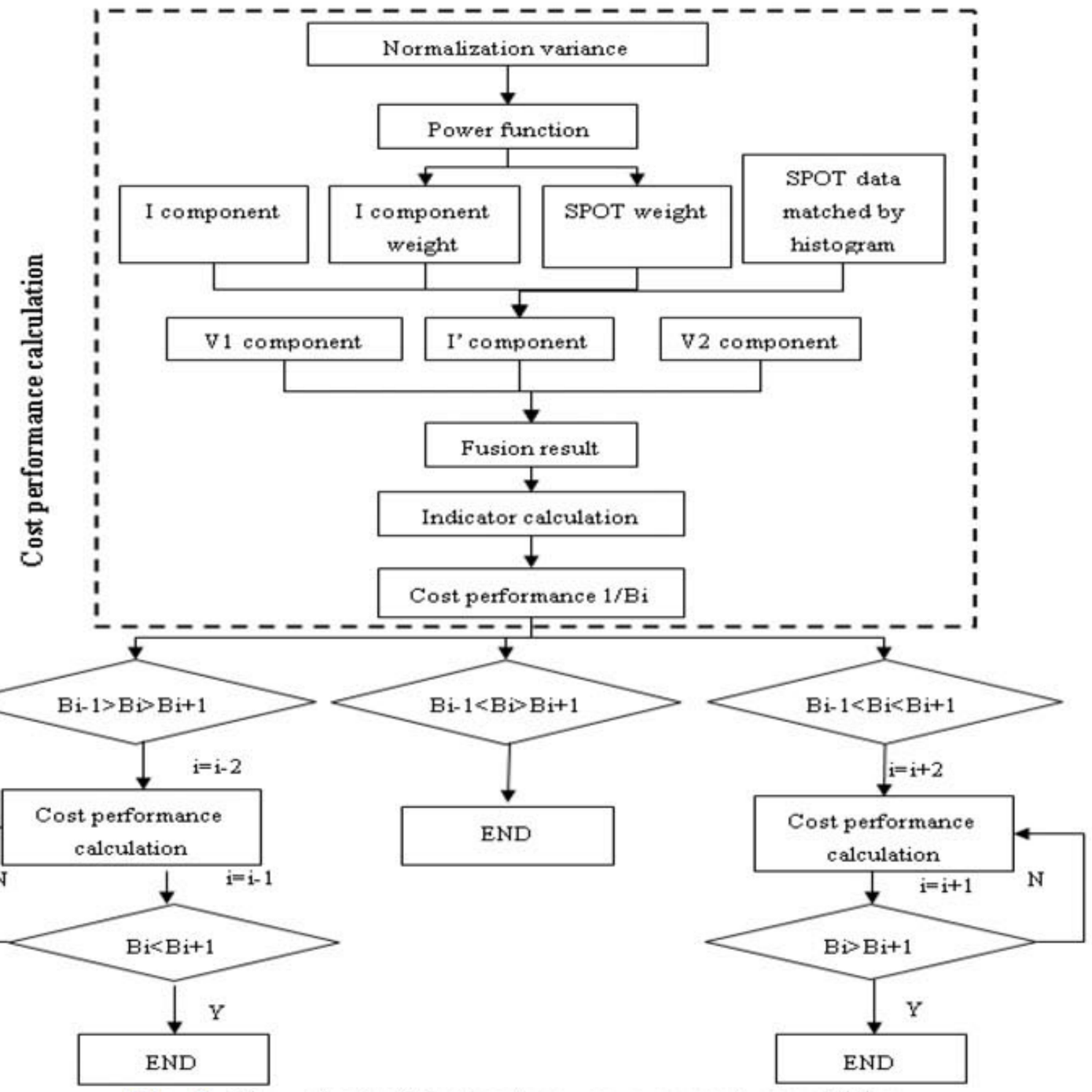

Fig. 8. Flow chart of the best power exponent acquisition

Based on the data analysis and calculation above, the optimal power exponent is obtained to be 1/24 by the IDL, and the experimental result of the cost performance is shown in **Table 2**.

Table 2. Applications in each class

Power exponent	Cost performance	Power exponent	Cost performance
1	-1.74479	1/50	-1.56869
1/23	-1.5425	1/75	-1.60684
1/24	-1.54247	1/100	-1.64904
1/25	-1.54279	1/125	-1.69199
1/26	-1.54303	1/150	-1.73483

4.3 Experimental results and discussions

A false color image which is composed of TM band 541 is chosen as the TM image. Both the SPOT image and the TM image come from the Institute of Remote Sensing Applications of Chinese Academy of Sciences with a spatial resolution of 838×838 . The IHS, HSV, PCA, SFIM, GS, Brovey and the proposed method are used to fuse the images [22, 30, 35-38]. The original images and fusion results are shown in **Fig. 9**. The comparison of the proposed algorithm and the traditional algorithms is tabulated in **Table 3**.

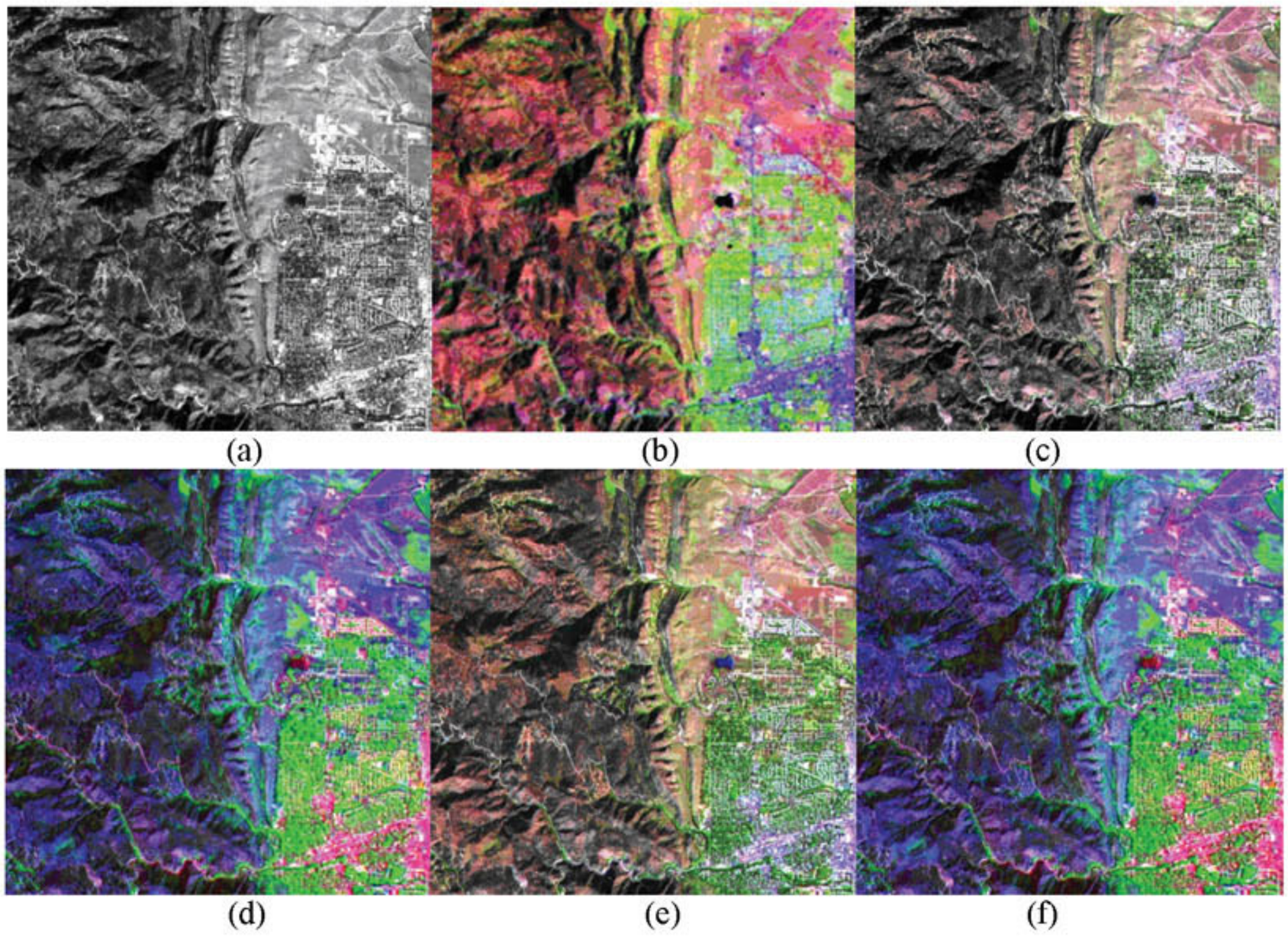

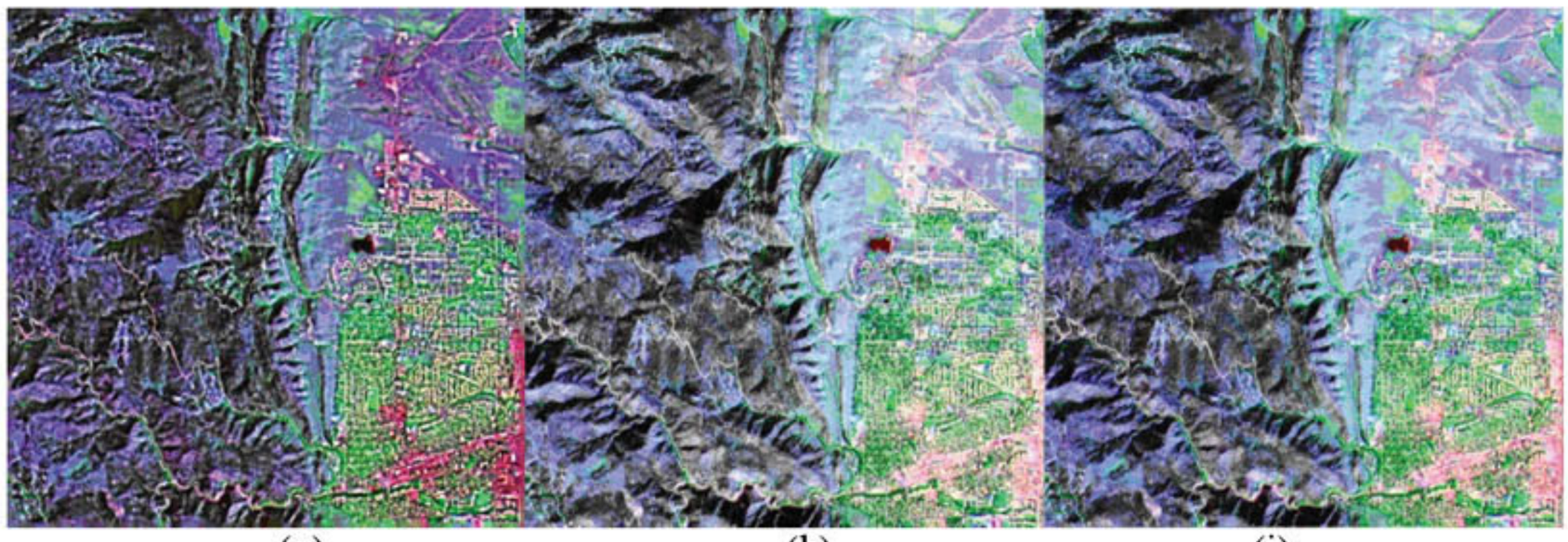

(g) (h) (i)

Fig. 9. The best fusion effect result of the images:(a) SPOT image; (b) False color image composed of TM band 5, 4, 1;(c) HSV transform; (d) PCA transform; (e) Brovey transform; (f) GS transform; (g) SFIM transform; (h) IHS transform; (i)The proposed algorithm $y = x^{1/24}$ fusion result coefficient.

Table 3. Comparison of the proposed algorithm and the traditional algorithm on the pertained quantitative fusion evaluation indices

method	S D	A G	I E	D D	D C	C C
TM	18.51	2.43	6.12	---	---	---
SPOT	15.09	4.08	5.80	---	---	---
HSV	41.02	8.72	7.16	39.33	0.40	0.68
PCA	18.46	4.6461	6.02	9.54	0.09	0.78
Brovey	18.34	4.45	5.26	10.16	0.08	0.73
GS	18.32	4.76	6.03	9.49	0.09	0.77
SFIM	19.61	6.54	6.21	4.41	0.04	0.87
IHS	34.57	9.33	7.09	21.81	0.24	0.55
$y = x^{1/24}$	29.83	7.73	6.88	16.87	0.18	0.72

Table 3 indicates that: (1) Compared with the original images, the fused images have improvements in all considered indices and result in better visual effect. (2) In terms of the standard deviation and entropy which reflect information richness, HSV transform is the best, which means images after HSV transform retain the most spectrum information. The proposed algorithm is only inferior to HSV and IHS algorithm, and superior to other algorithms. (3) In terms of averaged gradient, IHS transform is obviously superior to other algorithms, which means the detailed information of the fused images is enhanced to a large extent. The proposed algorithm is better than Brovey, PCA and GS transform in terms of averaged gradient. (4) In terms of the spectrum fidelity, SFIM is the best, which means the transformed image best matches the original image with less distortion. Low spectrum fidelity of IHS algorithm implies that it has poor spectrum fidelity. The proposed algorithm is only second to SFIM algorithm while better than other algorithms. (5) Brovey, PCA and GS transform provides similar detailed space information as well as the spectrum fidelity and results in similar fusion effects, which are all inferior to the proposed algorithm. (6) Compared with traditional IHS algorithm, the proposed IHS algorithm could not only provide high resolution, but also enhance the spectrum fidelity. As a result, the fusion effect can be drastically improved.

The experimental valuation indices have proven that the increase of the average gradient, standard deviation and entropy will result in the reduction of the spectrum fidelity (difference coefficient, distortion degree and correlation coefficient). The HSV and IHS algorithms focus on improving the standard deviation, average gradient and entropy, so it results in poor

distortion degree, difference coefficient and correlation coefficient. On the contrary, the PCA, Brovey, GS and SFIM algorithms improve the distortion degree, difference coefficient and correlation coefficient, at the cost of worsening other parameters. Such imbalance influences the fusion result while an appropriate power exponent with the highest cost performance as proposed in this paper could better balance these parameters.

Fig. 9 shows that the proposed algorithm could obtain the best result among all the results visually. The experimental results have proved that the proposed algorithm could provide a better balance between the spectrum fidelity and other indices, and an appropriate power exponent with the highest cost performance is very important for obtaining the best result of the fusion.

5. Conclusion

In this paper, an improved IHS transform fusion algorithm based on the local variance weighting scheme is proposed for remote sensing image. This algorithm links the local variance and weight images with the optimal power exponent that could yield the best cost performance. A better balance between the spectrum fidelity and other fusion indices can be established with the proposed method. The fusion process is performed by the Environment for Visualizing Images (ENVI) and the Interactive Data Language (IDL). Experiment result has demonstrated that the proposed algorithm could provide superior fused image on the pertained quantitative fusion evaluation indices. However, whether the power exponent is the best option for fusion needs further investigation.

References

[1] X. F. Wen, "Image fusion based on improved IHS transform with weighted average," in *Proc. of International Conference on Computational and Information Sciences (ICCIS)*, pp. 111-113, Chengdu, 2011. Article (CrossRef Link).

[2] F. A. Al-Wassai, N. V. Kalyankar, A. A. Al-Zuky, "The IHS transformations based image fusion," *Journal of Global Research in Computer Science*, vol. 2, no. 5, pp. 70-77, 2011. Article (CrossRef Link).

[3] E. M. Schetselaar, "Fusion by the IHS transform: Should we use cylindrical or spherical coordinates," *International Journal of Remote Sensing*, vol. 19, no. 4, pp. 759-765, 1998. Article (CrossRef Link).

[4] R. Redondo, F. Šroubek, S. Fischer, G. Cristóbal, "Multifocusimage fusion using the log-Gabor transform and a multisize windows technique," *Information Fusion*, vol. 10, no. 2, pp. 163-171, 2009. Article (CrossRef Link).

[5] M. Zribi, "Non-parametric and region-based image fusion with bootstrap sampling," *Information Fusion*, vol. 11, no. 2, pp. 85-94, 2010. Article (CrossRef Link).

[6] S. Daneshvar, H. Ghassemian, "MRI and PET image fusion by combiningIHS and retina-inspired models," *Information Fusion*, vol. 11, no. 2, pp. 114-123, 2010. Article (CrossRef Link).

[7] F. Al-Wassai, N. V. Kalyankar, and A. A. Al-Zaky, "Multisensor images fusion based on feature-level," *International Journal of Latest Technology in Engineering, Management and Applied Science*, vol. 1, no. 5, pp. 124-138, 2012. Article (CrossRef Link).

[8] R. Gharbia, A. T. Azar, A. E. Baz, A. E. Hassanien, Image Fusion Techniques in Remote Sensing. [online]: available: https://arxiv.org/abs/1403.5473. Article (CrossRef Link).

[9] T. Ranchin, L. Wald, M. Mangolini, "The ARSIS method: a general solution for improving spatial resolution of images by the means of sensor fusion," *Special Oil & Gas Reservoirs*, vol. 41, no. 2, pp. 358-361, 1996. Article (CrossRef Link).

[10] T. Ranchin, L. Wald, M. Mangolini, C. Penicand, "On the assessment of merging processes for the improvement of the spatial resolution of multispectral SPOT XS images," in *Proc. of the conference, Cannes, France, February 6-8, 1996, published by SEE/URISCA, Nice, France,* pp. 59-67, 1996. Article (CrossRef Link).
[11] A. A. Goshtasby, S. Nikolov, "Image fusion: advances in the state of the art," *Information Fusion*, vol. 8, no. 2, pp. 114-118, 2007. Article (CrossRef Link).
[12] T. M. Tu, W. C. Cheng, C. P. Chang, P. S. Huang, J. C. Chang, "Best tradeoff for high-resolution image fusion to preserve spatial details and minimize color distortion," *IEEE Geoscience and Remote Sensing Letters*, vol. 4, no. 2, pp. 302-306, 2007. Article (CrossRef Link).
[13] D. L. Hall, J. Llinas, "An introduction to multisensor data fusion," in *Proc. of the IEEE*, vol. 85, no. 1, pp. 6-23, 1997. Article (CrossRef Link).
[14] C. Pohl, J. L. Van Genderen, "Multisensor image fusion in remote sensing: concepts, methods and applications," *International Journal of Remote Sensing*, vol. 19, no. 5, pp. 823-854, 1998. Article (CrossRef Link).
[15] P. K. Varshney, "Multisensor data fusion," *Electronics and Communication Engineering Journal*, vol. 9, no. 6, pp. 245-253, 1997. Article (CrossRef Link).
[16] E. M. Schetselaar, "On preserving spectral balance in image fusion andits advantages for geological image interpretation," *Photogrammetric Engineering & Remote Sensing,* vol. 4, no. 2, pp. 925-934, 2001. Article (CrossRef Link).
[17] S. T. Li, J. T. Kwok, Y. N. Wang, "Using the discrete wavelet frame transform to merge landsat TM and SPOT panchromatic images," *Information Fusion*, vol. 3, no. 1, pp. 17-23, 2002. Article (CrossRef Link).
[18] Z. J. Wang, D. Ziou, C. Armenakis, D. R. Li, Q. Q. Li, "A comparativeanalysis of image fusion methods," *IEEE Transactions on Geoscience and Remote Sensing*, vol. 43, no. 6, pp. 1391-1402, 2005. Article (CrossRef Link).
[19] J. Lu, B. M. Zhang, Z. H. Gong, E. Li, H. Y. Liu, "The remote-sensingimage fusion based on GPU," *The International Archives of the Photogrammetry, Remote Sensing and Spatial Information Sciences*, Vol. 37, Part B7, pp. 1233-1238, Beijing 2008. Article (CrossRef Link).
[20] X. H. Yang, L. C. Jiao, "Fusion algorithm for remote sensing images based on nonsubsampled contourlet transform," *ACTA AUTOMATICA SINICA*, vol. 34, no. 3, pp. 274-281, 2008. Article (CrossRef Link).
[21] S. L. Hsu, P. W. Gau, I. L. Wu, J. H. Jeng, "Region-based image fusion with artificial neural network," *World Academy of Science, Engineering and Technology*, vol. 29, pp. 156-159, 2009. Article (CrossRef Link).
[22] W. J. Carper, T. W. Lilesand, R. W. Kieffer, "The use of Intensity-Hue-Saturation transformation for merging SPOT panchromatic and multispectral image data," *Photogrammetric Engineering and Remote Sensing*, vol. 56, no. 4, pp. 459-467, 1990. Article (CrossRef Link).
[23] M. González-Audícana, J. L. Saleta, R. G. Catalán, R. García, "Fusion of multispectral and panchromatic images using improved IHS and PCA mergers based on wavelet decomposition," *IEEE Transaction on Geoscience and Remote Sensing*, vol. 42, no. 6, pp.1291-1299, 2004. Article (CrossRef Link).
[24] Y. Zhang, G. Hong, "An IHS and wavelet integrated approach to improvepan-sharpening visual quality of natural colour IKONOS and Quick Bird images," *Information Fusion*, vol. 6, no. 3, pp. 225-234, 2005. Article (CrossRef Link).
[25] M. Choi, "A new intensity-hue-saturation fusion approach to image fusion with a tradeoff parameter," *IEEE Transactions on Geoscience and Remote Sensing*, vol. 44, no. 6, pp. 1672-1682, 2006. Article (CrossRef Link).
[26] T. M. Tu, P. S. Huang, C. L. Hung, C. P. Chang, "A fastintensity-hue-saturation fusion technique with spectral adjustment for IKONOS imagery," *IEEE Geoscience and Remote Sensing Letter*, vol. 1, no. 4, pp. 309-312, 2004. Article (CrossRef Link).
[27] I. De, B. Chanda, "A simple and efficient algorithm for multifocus image fusion using morphological wavelets," *Signal Processing*, vol. 86, no. 5, pp. 924-936, 2006. Article (CrossRef Link).

[28] M. N. Do, M. Vetterli, "The contourlet transform: an efficient directional multire solution image representation," *IEEE Transactions on Image Processing*, vol. 14, no. 12, pp. 2091-2106, 2005. Article (CrossRef Link).
[29] R. A. Schowengerdt, "Reconstruction of multi-spatial, multispectral image data using spatial frequency content," *Photogrammetric Engineering & Remote Sensing*, vol. 46, no. 10, pp. 1325-1334, 1980. Article (CrossRef Link).
[30] P. S. Chavez, Jr., S. C. Sides, J. A. Anderson, "Comparison of three different methods to merge multire solution data: Landsat TM and SPOT Panchromatic," *Photogrammetric Engineering & Remote Sensing*, vol. 57, no. 3, pp. 295-303, 1991. Article (CrossRef Link).
[31] J. G. Liu, "Smoothing Filter-based Intensity Modulation: a spectral preserve image fusion technique for improving spatial details," *International Journal of Remote Sensing*, vol. 21, no. 18, pp.3461-3472, 2000. Article (CrossRef Link).
[32] J. R. Jensen, *Introductory digital image processing: a remote sensing perspective*, Prentice Hall Press, 2005. Article (CrossRef Link).
[33] O. Gungor, J. Shan, "Colour-based and criteria-based methods for image fusion," *The International Archives of the Photogrammetry, Remote Sensing and Spatial Information Sciences*, Vol. 37, Part B7, pp. 1057-1064, Beijing, 2008. Article (CrossRef Link).
[34] B. A. Harrison, D. L. B. Jupp, *MicroBRIAN resource manual: Introduction to image processing*, CSIRO Australia, Division of Water Resources Press, 1990. Article (CrossRef Link).
[35] B. Garguet-Duport, J. Girel, J.-M. Chassery, G. Pautou, "The use of multiresolution analysis and wavelets transform for merging SPOT panchromatic and multispectral image data," *Photogrammetric Engineering & Remote Sensing*, vol. 62, no. 9, pp. 1057-1066, 1996. Article (CrossRef Link).
[36] C. Pohl, J. L. Van Genderen, "Multisensor image fusion in remote sensing: concepts, methods and applications," *International Journal of Remote Sensing*, vol. 19, no. 5, pp. 823-854, 1998. Article (CrossRef Link).
[37] J. G. Liu, "Smoothing filter-based intensity modulation: a spectral preserve image fusion technique for improving spatial details," *International Journal of Remote Sensing*, vol. 21, no. 18, pp.3461-3472, 2000. Article (CrossRef Link).
[38] D. G. Clayton, "Gram-Schmidt orthogonalization," *Applied Statistics*, vol. 20, no. 3, pp. 335-338, 1971. Article (CrossRef Link).

Chao Deng received the B.Sc. degree and the M. Sc. degree in communication engineering from Jilin University, China, in 2002 and 2005. He then received the Ph. D. degrees in Changchun Institute of Optics, Fine Mechanics and Physics, Chinese Academy of Sciences in 2008. He is currently an associate professor with the School of Physics and Electronic Information Engineering, Henan Polytechnic University, Jiaozuo China. His research interests include image processing and signal processing. Email: super@hpu.edu.cn.

Zhiheng Wang received the BS degree in Mechatronical Engineering from Beijing Institute of Technology, China, in 2004, and the Ph.D from the Institute of Automation, Chinese Academy of Sciences, China, in 2009. Currently, he is an Associate Professor at School of Computer Science and Technology, Henan Polytechnic University, China, serves as the "Chinese Science" and "Automation Technology" expert reviewers. His research interests include computer vision and innovation research. He Published in SCI / EI included 20 papers, authorized national invention patents 9. Email: wzhenry@eyou.com.

Xingwang Li received the B.Sc. degree in communication engineering from Henan Polytechnic University, China, in 2007. He then received the M. Sc. degree from the National Key Laboratory of Science and Technology on Communications at University of Electronic Science and Technology of China (UESTC) and Ph. D. degrees in communication and information system from the State Key Laboratory of Networking and Switching Technology at Beijing University of Posts and Telecommunications (BUPT). He is currently a lecturer with the School of Physics and Electronic Information Engineering, Henan Polytechnic University, Jiaozuo China. His research interests include massive MIMO, hardware constrained communication, FSO communications, and performance analysis of fading channels. Email: lixingwangbupt@gmail.com

Huina Li received the B.Sc. degree and M. Sc. degree in communication engineering from Henan Polytechnic University, China, in 2009 and 2012. She is currently a lecturer with the College of Computer Science and Technology, Xuchang University, Jiaozuo China. Her research interests include image processing and signal processing. Email: lihuina851013@163.com.

Charles Casimiro Cavalcante received the B.Sc and M.Sc in Electrical Engineering from the Federal University of Cear (UFC), Brazil, in 1999 and 2001, respectively, and the Ph.D. degree from the University of Campinas (UNICAMP), Brazil, in 2004. He has held a grant for Scientific and Technological Development from 2004 to 2007 and since March 2009 he has a grant of Scientific Research Productivity both from the Brazilian Research Council (CNPq). From March 2007 to November 2008 he was a Visiting Professor at Teleinformatics Engineering Department of UFC and since November 2008 he is an Assistant Professor at the same department and university holding the Statistical Signal Processing chair. From August 2014 to July 2015 he was a Visiting Assistant Professor at the Department of Computer Science and Electrical Engineering (CSEE) from University of Maryland, Baltimore County (UMBC) in the United States. He has been working on signal processing strategies for communications where he has several papers published in journal and conferences, has authored three international patents and he has worked on several funded research projects on the signal processing and wireless communications areas. He is also a co-author of the book Unsupervised Signal Processing: Channel Equalization and Source Separation, published by CRC Press. He is a researcher of the Wireless Telecommunications Research Group (GTEL) where he leads research on signal processing and wireless communications. Dr. Cavalcante is a Senior Member of the IEEE and Senior Member of the Brazilian Telecommunications Society (SBrT). His main research interests are in signal processing for communications, blind source separation, wireless communications, and statistical signal processing.